Seasonal variation of eddy kinetic energy of the North Pacific Subtropical Countercurrent simulated by an eddy-resolving OGCM

Yign Noh,[1] Bo Young Yim,[1] Sung Hyup You,[2,3] Jong Hwan Yoon,[2] and Bo Qiu[4]

Received 18 December 2006; revised 3 February 2007; accepted 14 February 2007; published 3 April 2007.

[1] The seasonal variation of eddy kinetic energy (EKE) of the North Pacific Subtropical Countercurrent (STCC) was investigated by analyzing the data from an eddy-resolving OGCM with the horizontal resolution 1/12° in comparison with satellite altimetry data. Although the annual cycle of simulated EKE of the whole STCC domain showed agreement with satellite data, with a maximum in spring and a minimum in fall, it revealed latitudinal dependence; that is, near 19°N the EKE level is higher in summer than in winter, but it is higher in winter than in summer north of 20°N. The OGCM also reproduced two branches of the STCC, which affect the EKE variation. The variation of EKE level was shown to be closely related to the growth rate of baroclinic eddies. The simulated zonal velocity is much larger than climatological value, thus allowing much faster growth of baroclinic eddies. **Citation:** Noh, Y., B. Y. Yim, S. H. You, J. H. Yoon, and B. Qiu (2007), Seasonal variation of eddy kinetic energy of the North Pacific Subtropical Countercurrent simulated by an eddy-resolving OGCM, *Geophys. Res. Lett.*, *34*, L07601, doi:10.1029/2006GL029130.

1. Introduction

[2] Major advances have been made recently in the understanding of mesoscale variability of the ocean thanks to the availability of satellite altimetry data and eddy-resolving ocean general circulation models (OGCM) [e.g., *Stammer*, 1997; *Qiu*, 1999; *Smith et al.*, 2000; *Ducet and Le Traon*, 2001; *Brachet et al.*, 2004].

[3] In particular, *Qiu* [1999] has found from the analysis of TOPEX/Poseidon (T/P) satellite data that the eddy kinetic energy (EKE) of the North Pacific Subtropical Countercurrent (STCC), which flows eastward near the center of the western North Pacific subtropical gyre, shows a well-defined annual cycle with a maximum in April/May and a minimum in December/January with the amplitude exceeding 200 cm^2s^{-2}. He also showed that the seasonal modulation of EKE is a manifestation of baroclinic instability.

[4] Meanwhile, several observation data analyses suggested that the STCC is actually made of multiple zonal bands of eastward currents [*Hasunuma and Yoshida*, 1978; *White and Walker*, 1985; *Aoki et al.*, 2002; *Kobashi and Kawamura*, 2002]. For example, *Aoki et al.* [2002] and *Kobashi and Kawamura* [2002] suggested two branches of the STCC; one along 24°N from 130°E to 160°W and the other along 20°N from about 150°E to the west of Hawaii Island. The latter is often called separately as the Hawaiian Lee Countercurrent [*Qiu et al.*, 1997]. They also found that each branch has a different seasonal variation pattern.

[5] In the present paper we examined whether such an annual cycle of the EKE of the STCC is reproduced in an OGCM, together with the corresponding realistic distributions of velocity and temperature. It is also interesting to see how the EKE variation is related to two branches of the STCC. Furthermore, the OGCM data provides us information on the relation between EKE and the subsurface oceanic structure, which is unavailable from satellite data.

2. Model

[6] The OGCM used in this study (RIAMOM) is a multilevel model with a free surface that solves hydrostatic primitive equations. The model covers from 95°E to 70°W in longitude and from 50°S to 65°N in latitude. The horizontal grid interval is 1/12° in both latitudinal and longitudinal directions, and there are 70 vertical levels, with 9 levels in the upper 90 m. Note that the horizontal resolution of the OGCM must be smaller than 1/10° in order to resolve mesoscale eddies globally [*Smith et al.*, 2000]. The advection of momentum is treated by the generalized Arakawa scheme [*Ishizaki and Motoi*, 1999], which conserves potential enstrophy as well as kinetic energy. It also uses an improved advection scheme of tracers by *Webb et al.* [1998] and the biharmonic diffusion for both momentum and tracers. The vertical mixing is improved by the Noh scheme, which was shown to reproduce more realistic subsurface stratification [*Noh and Kim*, 1999; *Noh et al.*, 2002]. The detailed explanation and the general performance of the model is given by *You* [2005].

[7] The model was started from the state of rest with climatological temperature and salinity distributions by WOA94 [*Levitus and Boyer*, 1994; *Levitus et al.*, 1994], and was forced by the climatological forcing of wind stress and heat flux from the NCEP reanalysis data. The combined boundary condition using both the climatological flux and a restoring term was used for the heat flux, similar to *Noh et al.* [2002], and the restoring boundary condition was used for salinity. At the southern boundary, temperature and salinity were restored to climatological values. The model was integrated for 25 years, which is long enough for the upper ocean to reach quasi-equilibrium. Three-dimensional

[1]Department of Atmospheric Sciences/Global Environmental Laboratory, Yonsei University, Seoul, South Korea.
[2]Research Institute for Applied Mechanics, Kyushu University, Fukuoka, Japan.
[3]Now at Marine Meteorology and Earthquake Research Laboratory, Meteorological Research Institute, Seoul, South Korea.
[4]Department of Oceanography, University of Hawaii at Manoa, Honolulu, Hawaii, USA.

0094-8276/07/2006GL029130$05.00

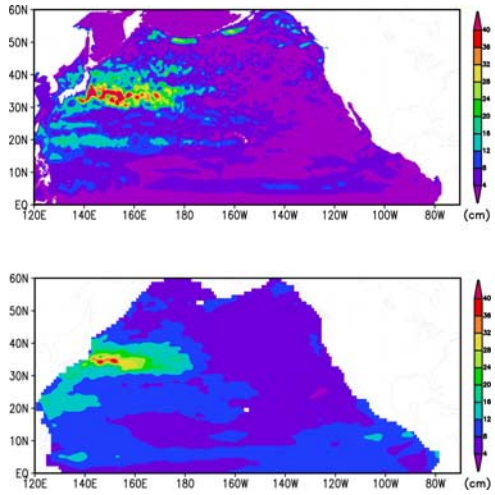

Figure 1. Map of the rms sea surface height anomaly (SSHA) variability in the North Pacific from the (top) OGCM and (bottom) T/P.

prognostic variables were archived every model day of the last year, and were used for analysis.

3. Results

[8] Figure 1 compared the rms sea surface height anomaly (SSHA) in the Pacific Ocean, obtained from OGCM and satellite data. The gradient of SSHA h', where h' represents an anomaly from the annual mean SSH, is related to the horizontal velocity of mesoscale eddies $\mathbf{u}_g'$ by geostrophic balance, i.e., $\mathbf{u}_g' = (g/f)\mathbf{k} \times \nabla h'$, and thus to EKE $[\langle u_g'^2 \rangle + \langle v_g'^2 \rangle]/2$. The satellite data has the horizontal resolution of 0.25°, and was obtained at 10 day intervals. A similar pattern appears from both data with high SSHA variability in the regions of the Kuroshio, the North Equatorial Countercurrent, and the STCC, although the SSHA of the Kuroshio is stronger and broader than satellite data. Higher SSHA variability from satellite data in the regions of low variability, such as the eastern basin, is mainly due to higher signal error [*Smith et al.*, 2000].

[9] The annual cycle of EKE in the STCC region 19°–25°N, 135°E–175°W also shows agreement between two data with a maximum in spring and a minimum in fall, although a phase lead of about 2 months appears in the

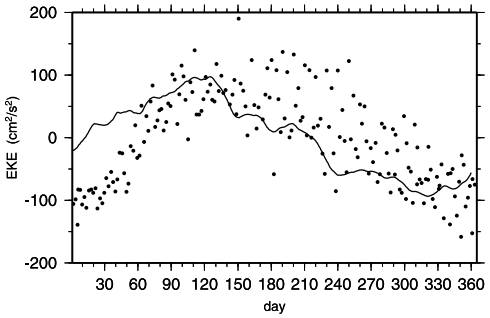

Figure 2. Annual cycle of the EKE anomalies of the STCC inferred from the OGCM (solid line) and T/P (dots). The data from T/P are from October 1992 to December 1997.

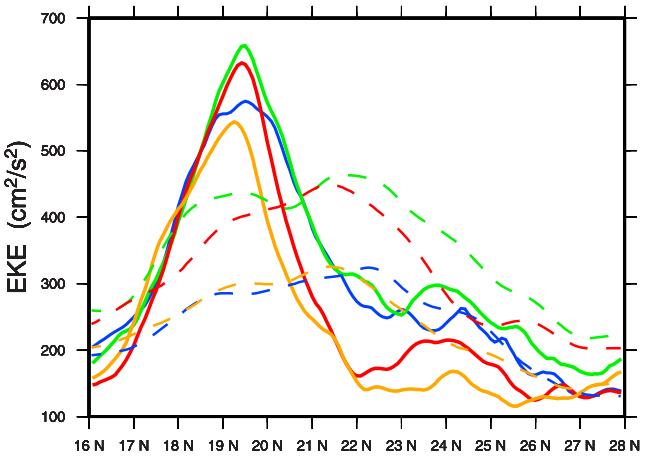

Figure 3. Meridional variation of the zonally averaged EKE distributions (135°E–175°W) in four seasons from the OGCM (solid line) and T/P (dashed line) (JFM: winter (blue), AMJ: spring (green), JAS: summer (red), and OND: fall (yellow)).

OGCM results (Figure 2). Both the stronger SSHA of the western boundary current and the phase difference in the annual cycle of EKE, in comparison with satellite data, were also found in the Atlantic Ocean [*Brachet et al.*, 2004].

[10] Meanwhile, the zonally averaged EKE shows a stronger meridional variation in OGCM results than in satellite data, with the higher EKE level near 19°N (Figure 3). Weaker meridional variation in the observation data may be affected by the existence of interannual variations. Furthermore, OGCM results reveal that the seasonal variation pattern of EKE differs depending on latitude. Near 19°N the EKE level is higher in summer than in winter, whereas north of 20°N it is higher in winter than in summer. On the other hand, the EKE level in spring is always higher than that in fall in the whole domain.

[11] In order to investigate the oceanic structure associated with the EKE variation, we examined the temperature distribution along 150°E in comparison with the climatology (Figure 4). The simulated result reproduces well the general features of climatological temperature distribution at all seasons. Furthermore, it reproduces two subsurface fronts predicted from previous hydrographic data analysis [*Aoki et al.*, 2002; *Kobashi and Kawamura*, 2002], a stronger one along 18–20°N and a weaker one along 24–26°N, corresponding to southern and northern branches of the STCC, respectively.

[12] The corresponding distribution of zonal velocity reveals multiple zonal bands of alternating zonal velocity, including two branches of the STCC (Figure 5). The weaker northern branch along 24–26°N is weakest in September and December and the stronger southern branch along 18–20°N is weakest in March, in agreement with *Kobashi and Kawamura* [2002]. The zonal velocity is also consistent with the field observation (>20 cms^{-1}) [*Roden*, 1998; *Aoki et al.*, 2002]. On the other hand, it is in contrast to a single zonal band of the STCC estimated from climatological hydrology that is much weaker (<10 cms^{-1}), shallower (<100 m), and wider (>500 km) [see *Qiu*, 1999, Figure 9]. Note that the averaging process removes fluctuation in the temperature distribution in climatological data, as shown in

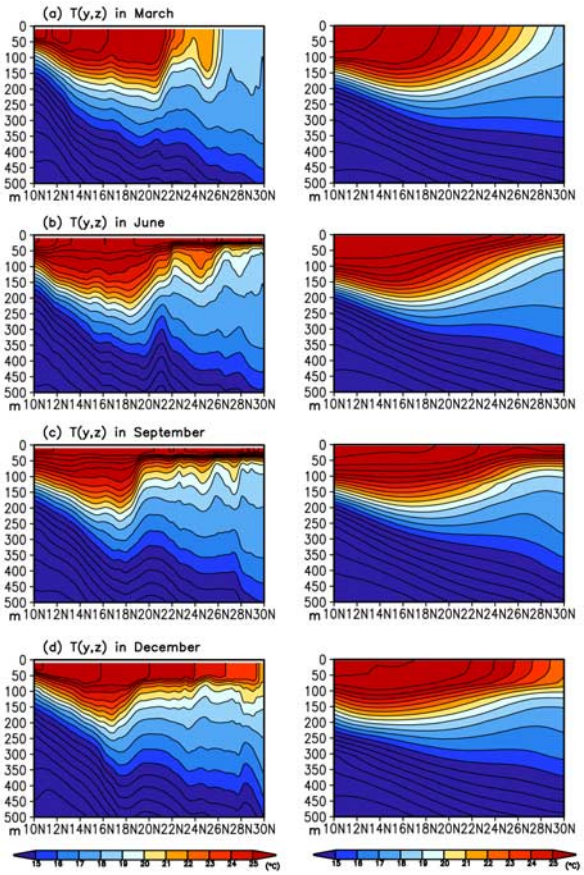

Figure 4. Temperature distribution at 150°E at each season from the (left) OGCM and (right) climatological data.

Figure 4, and thus decreasing the zonal velocity. Figure 5 also confirms the existence of alternating zonal jets in the global ocean found recently in the satellite and high resolution OGCM data [*Nakano and Hasumi*, 2005; *Maximenko et al.*, 2005].

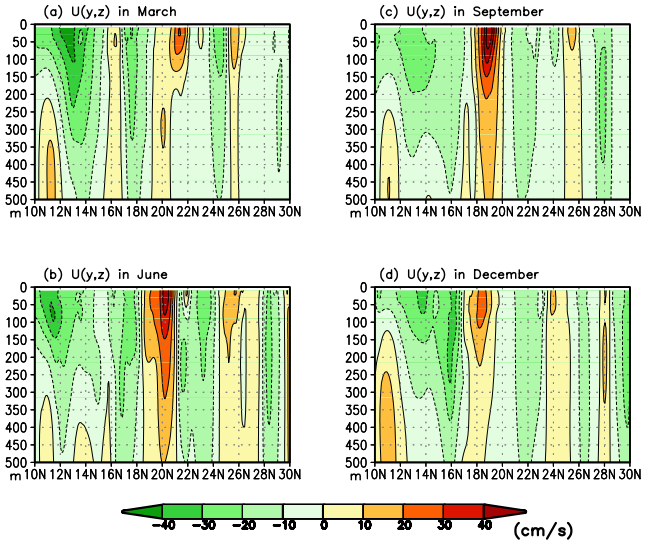

Figure 5. Zonal velocity distribution at 150°E at each season from the OGCM.

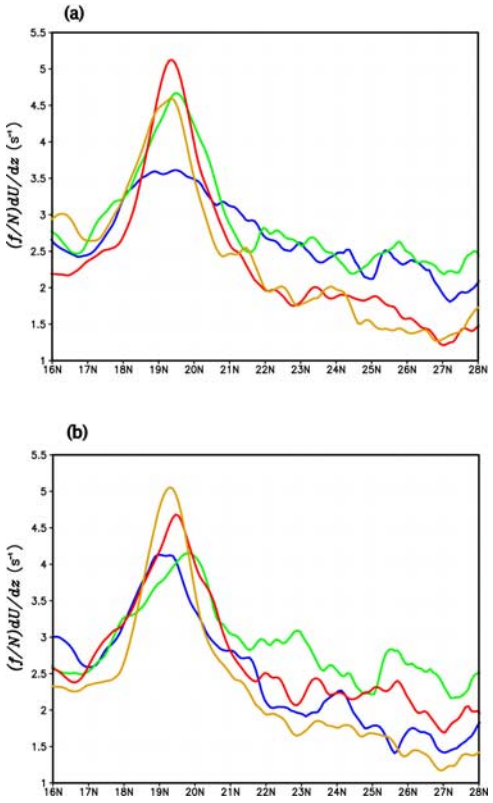

Figure 6. Meridional variation of the zonally averaged value of $(f/N)dU/dz$ (135°E–175°W) at each season from the OGCM. (a) JFM: winter (blue), AMJ: spring (green), JAS: summer (red), and OND: fall (yellow). (b) Two-month phase-lead: NDJ (blue), FMA (green), MJJ (red), ASO (yellow).

[13] It has been known that mesoscale eddies are generated primarily by baroclinic instability [*Stammer*, 1997; *Qiu*, 1999]. Therefore, we examined the meridional distribution of the growth rate of baroclinic eddies $(f/N)dU/dz$ [*Charney*, 1947; *Eady*, 1949] at each season, where both the Brunt-Väisälä frequency N and the vertical shear of zonal velocity dU/dz were calculated over the depth of 400 m, and the Coriolis parameter f was fixed. It shows a good correlation with the EKE variation in Figure 3 in the meridional distribution and in the seasonal variation (Figure 6a). In particular, near 19°N (north of 20°N), the value of $(f/N)dU/dz$ is high in summer (winter) and low in winter (summer), in accord with the EKE variation. It suggests that stronger zonal velocity of the southern branch of the STCC makes the EKE level near 19°N higher in summer. Meanwhile, the weaker stratification appears to be mainly responsible for the enhancement of the EKE level north of 20°N in winter. The meridional distribution of the vertical velocity shear only, dU/dz, as used by *Stammer* [1997] and *Qiu* [1999], could not reproduce the seasonal variation north of 20°N properly, suggesting the importance of stratification for baroclinic instability in this region (not shown). The values of $(f/N)dU/dz$ near 19°N in spring and fall are comparable, however, although the EKE level is higher in spring. The reason is not clear, but it can be attributed to other sources of EKE such as barotropic instability.

[14] On the other hand, the meridional variation of $(f/N)dU/dz$ with a phase-lead of 2 months shows poor correlation with Figure 3 (Figure 6b), suggesting that there is no phase lag between baroclinic instability and EKE. It does not agree with the result based on the satellite and climatological data [*Qiu*, 1999; *Kobashi and Kawamura*, 2002], where 2 month phase-lag appears in the annual cycle of EKE. We can expect that the time scale for the growth of baroclinic eddies is much shorter here, because dU/dz is much larger than the climatological one.

4. Conclusion

[15] We have shown that an eddy-resolving OGCM reproduces well the observed annual cycle of the EKE level of the STCC, a maximum in spring and a minimum in fall, along with the realistic distributions of temperature and velocity.

[16] At the same time, the simulation result reveals several new insights regarding the mesoscale variability of the STCC. The seasonal variation of EKE shows a different pattern depending on latitude. Near 19°N the EKE level is higher in summer than in winter, but it is higher in winter than in summer north of 20°N. The OGCM also reproduced two branches of the STCC, which affect the EKE variation. The variation of EKE level was shown to be closely related to the growth rate of baroclinic eddies $(f/N)dU/dz$. The simulated zonal velocity is much larger than climatological value, thus allowing much faster growth of baroclinic eddies.

[17] Meanwhile, the simulated EKE along the southern branch of the STCC and the Kuroshio is higher than satellite data, and a phase difference appears between the two seasonal variations of EKE. This discrepancy is possibly attributed to the coarser resolution of satellite data, which cannot detect smaller scale eddies with faster growth rate, but more studies on both satellite data and the OGCM are required in the future study to resolve it. Finally, we should mention that, although we used the T/P data in order to avoid confusion in comparing the results with those of *Qiu* [1999], the difference from the updated AVISO combined satellite data set is insignificant for the mesoscale variability of the STCC region.

[18] **Acknowledgments.** This work was supported by Korean Ministry of Environment as 'The Eco-technopia 21 project', KOSEF (SRC and International Cooperative Research), and KRF (KRF-2003-015-C00684). Simulation was carried out by using the Earth Simulator in Japan.

References

Aoki, Y., T. Suga, and K. Hanawa (2002), Subsurface subtropical fronts of the North Pacific as inherent boundaries in the ventilated thermocline, *J. Phys. Oceanogr.*, *32*, 2299–2311.

Brachet, S., P. Y. Le Traon, and C. Le Provost (2004), Mesoscale variability from a high-resolution model and from altimeter data in the North Atlantic Ocean, *J. Geophys. Res.*, *109*, C12025, doi:10.1029/2004JC002360.

Charney, J. G. (1947), The dynamics of long waves in a baroclinic westerly current, *J. Meteorol.*, *4*, 135–163.

Ducet, N., and P. Y. Le Traon (2001), A comparison of surface eddy kinetic energy and Reynolds stresses in the Gulf Stream and the Kuroshio Current systems from merged TOPEX/Poseidon and ERX-1/2 altimetric data, *J. Geophys. Res.*, *106*, 16,603–16,622.

Eady, E. T. (1949), Long waves and cyclonic waves, *Tellus*, *1*, 33–52.

Hasunuma, K., and K. Yoshida (1978), Splitting the subtropical gyre in the western North Pacific, *J. Oceanogr. Soc. Jpn.*, *34*, 160–172.

Ishizaki, H., and T. Motoi (1999), Reevaluation of the Takano-Oonishi scheme for momentum advection of bottom relief in ocean models, *J. Atmos. Oceanic Technol.*, *16*, 1994–2010.

Kobashi, F., and H. Kawamura (2002), Seasonal variation and instability nature of the North Pacific Subtropical Countercurrent and the Hawaiian Lee Countercurrent, *J. Geophys. Res.*, *107*(C11), 3185, doi:10.1029/2001JC001225.

Levitus, S., and T. P. Boyer (1994), *World Ocean Atlas 1994*, vol. 4, *Temperature*, *NOAA Atlas NESDIS 4*, 117 pp., Natl. Oceanic and Atmos. Admin., Silver Spring, Md.

Levitus, S., R. Burgett, and T. P. Boyer (1994), *World Ocean Atlas 1994*, vol. 3, *Salinity*, *NOAA Atlas NESDIS 3*, 99 pp., Natl. Oceanic and Atmos. Admin., Silver Spring, Md.

Maximenko, N. A., B. Bang, and H. Sasaki (2005), Observational evidence of alternating zonal jets in the world ocean, *Geophys. Res. Lett.*, *32*, L12607, doi:10.1029/2005GL022728.

Nakano, H., and H. Hasumi (2005), A series of zonal jets embedded in the broad zonal flows in the Pacific obtained in eddy-permitting ocean general circulation models, *J. Phys. Oceanogr.*, *35*, 474–488.

Noh, Y., and H. J. Kim (1999), Simulations of temperature and turbulence structure of the oceanic boundary layer with the improved near-surface process, *J. Geophys. Res.*, *104*, 15,621–15,634.

Noh, Y., C. J. Jang, T. Yamagata, P. C. Chu, and C. H. Kim (2002), Simulation of more realistic upper ocean process from an OGCM with a new ocean mixed layer model, *J. Phys. Oceanogr.*, *32*, 1284–1507.

Qiu, B. (1999), Seasonal eddy field modulation of the North Pacific Subtropical Countercurrent: TOPEX/Poseidon observations and theory, *J. Phys. Oceanogr.*, *29*, 2471–2486.

Qiu, B., D. Koh, C. Lumpkin, and P. Filament (1997), Existence and formation mechanism of the North Hawaiian Ridge Current, *J. Phys. Oceanogr.*, *27*, 431–444.

Roden, G. I. (1998), Upper ocean thermohaline, oxygen, nutrients, and flow structure near the data line in the summer of 1993, *J. Geophys. Res.*, *103*, 12,919–12,940.

Smith, R. D., M. E. Maltrud, F. O. Bryan, and M. W. Hecht (2000), Numerical simulation of the North Atlantic Ocean at 1/10°, *J. Phys. Oceanogr.*, *30*, 1531–1561.

Stammer, D. (1997), Global characteristics of ocean variability estimated from regional TOPEX/Poseidon altimeter measurements, *J. Phys. Oceanogr.*, *27*, 1743–1769.

Webb, D. J., B. A. de Cuevas, and C. S. Richimond (1998), Improved advection scheme for ocean models, *J. Atmos. Oceanic Technol.*, *15*, 1171–1187.

White, W. B., and A. E. Walker (1985), The influence of the Hawaiian Archipelago upon the wind-driven subtropical gyre in the western North Pacific, *J. Geophys. Res.*, *90*, 7061–7074.

You, S. H. (2005), A numerical study of the Kuroshio System southwest of Japan, Ph.D. thesis, Kyushu Univ., Fukuoka, Japan.

Y. Noh and B. Y. Yim, Department of Atmospheric Sciences/Global Environmental Laboratory, Yonsei University, 134 Shinchon-Dong, Seodaemun-gu, Seoul 120-749, South Korea. (noh@yonsei.ac.kr)

B. Qiu, Department of Oceanography, University of Hawaii at Manoa, 1000 Pope Road, Honolulu, HI 96822, USA.

J. H. Yoon, Research Institute for Applied Mechanics, Kyushu University, Fukuoka, Japan.

S. Y. You, Marine Meteorology and Earthquake Research Laboratory, Meteorological Research Institute, Seoul, South Korea.